HHS Public Access

Author manuscript

Nanomedicine. Author manuscript; available in PMC 2019 June 01.

Published in final edited form as:

Nanomedicine. 2018 June ; 14(4): 1301–1313. doi:10.1016/j.nano.2018.03.010.

Concomitant Delivery of Paclitaxel and NuBCP-9 peptide for synergistic enhancement of cancer therapy

Dikshi Gupta, PhD[a,*], **Manoj Kumar, PhD**[a], **Priyanka Tyagi, PhD**[a], **Sumeet Kapoor, PhD**[a], **Amit Tyagi, PhD**[b], **Tarani Kanta Barman, MVSc**[a], **Surender Kharbanda, PhD**[c], **Donald Kufe, MD**[c], and **Harpal Singh, PhD**[a,*]

[a]Centre for Biomedical Engineering, Indian Institute of Technology, HauzKhas, New Delhi, India

[b]Institute of Nuclear Medicine & Allied Sciences, DRDO, Timarpur, Delhi, India

[c]Department of Medical Oncology, Dana-Farber Cancer Institute Harvard Medical School, Boston, MA, USA

Abstract

Paclitaxel (PTX) is a microtubule inhibitor administered as an albumin-bound nanoformulation for the treatment of breast cancer. However, the effectiveness of PTX is limited by resistance mechanisms mediated in part by upregulation of the anti-apoptotic BCL-2 and P-glycoprotein (P-gp). Present investigation was designed to study the synergistic potential of NuBCP-9 and PTX loaded polymeric nanoparticles to minimize the dose and improve the efficacy and safety. PTX and NuBCP-9 loaded polylactic acid–polyethylene glycol-polypropylene glycol-polyethylene glycol [PLA-(PEG-PPG-PEG)] nanoparticles were prepared by double emulsion solvent evaporation method. PTX and NuBCP-9 loaded NPs displayed an average size of 90 nm with spherical morphology. PTX and NuBCP-9 dual loaded NPs reduced IC_{50} by ~40-fold and acted synergistically. Treatment of the syngeneic EAT mice with PTX-NuBCP-9/NPs resulted in improved efficacy than that alone treated mice. Overall, the concomitant delivery PTX and NuBCP-9 loaded NPs showed superior activity than that of PTX and NuBCP-9 alone treated mice.

Keywords

Paclitaxel; *nab*-paclitaxel; polymeric nanoparticles; NuBCP-9; BCL-2

Paclitaxel (PTX) is a widely used chemotherapeutic agent for the treatment of breast cancer and other solid tumors. It is administered in a solvent formulation or in albumin nanoparticles as *nab*-paclitaxel (Abraxane).[1–3] PTX stabilizes the microtubules from disassembly by binding to tubulins, locking the microtubules in a polymerized state and thereby inducing cell cycle arrest.[4–9] PTX also inhibits the anti-apoptotic BCL-2 protein,

*Corresponding authors: gupta.dikshi@gmail.com (D. Gupta), harpal@cbme.iitd.ac.in, harpal2000@yahoo.com (H. Singh).

Potential conflict of interest: The authors declare competing financial interests: S.K., D.K. and H.S. hold equity in NanoProteagen. The other authors disclosed no potential conflicts of interest. NanoProteagen has initiated preclinical development of PTX-NPs for potential clinical development in future.

Appendix A. Supplementary data

Supplementary data to this article can be found online at https://doi.org/10.1016/j.nano.2018.03.010.

and induces apoptosis by activation of the intrinsic mitochondrial pathway in cancer cells.[9] Taxol (cremophor based formulation), *Nab*-paclitaxel is approved for the treatment of metastatic breast cancer, locally advanced or metastatic non-small cell lung cancer (NSCLC) and metastatic pancreatic cancer.[10] However, PTX cremaphore formulation and *nab*-paclitaxel alone are not effective in drug resistance cancer often conferred by the anti-apoptotic BCL-2 proteins.[2,11–12]

The co-delivery of anti-cancer agents in nanoparticles (NPs) has provided promising opportunities for improving efficacy, decreasing off target toxicities and abrogating the development of resistance. PTX has been co-administered with doxorubicin using micelles of stearate-grafted chitosan oligosaccharide (CSO-SA).[13] However, its clinical use is limited due to the toxicity associated with small molecules. PEG-block-PLA (PEG-b-PLA) micelles have been used to deliver multiple drugs, including the combination of PTX and heat shock protein 90 (HSP-90) inhibitor 17-allylamino-17-demethoxygeldanamycin (17-AAG).[14] PTX and a BCL-2 targeted siRNA have also been incorporated into cationic core shell nanoparticles for breast cancer treatment.[15] In certain NP formulations, the effective dose of chemotherapeutic agents was reduced and adverse events were minimized, indicating that the strategy of co-delivering agents may improve efficacy as compared to administering drug alone.-[16–18] Experimental studies have also demonstrated that Pluronic® block copolymers sensitize MDR cells, resulting in an increase in the cytotoxic activity of anthracyclines and other cytotoxic drugs by 2 to 3 orders of magnitude.[19] Pluronics are known to be P-gp inhibitors, can block the drugs to efflux out from the cells.[20]

NuBCP-9 is a highly promising anticancer peptide, which selectively induces apoptosis of cancer cells by exposing the BCL-2 BH3 domain and blocking the BCL-xL survival function.[21] NuBCP-9 was linked to D-Argoctamer r8 for intracellular delivery, a modification that has been reported to decrease selectivity by inducing BCL-2-independent cell killing involving membrane disruption.[22] Our group recently reported the sustained delivery of L-NuBCP-9 in novel polymeric tetra-block PLA–PEG-PPG-PEG NPs that was effective in inducing significant regression of MCF-7 cancer cells in syngeneic BALB/c Ehrlich ascites tumor (EAT) model.[23] These findings opened up the possibility that the co-delivery of PTX and NuBCP-9 in polymeric nanoparticles could offer improved anti-tumor activity as compared to stand alone. In this study, PLA was conjugated with PEG-PPG-PEG (Pluronic F127) to form tetrablock copolymeric nanoparticles for the encapsulation and concomitant delivery of PTX and NuBCP-9 peptide with an aim to lower the toxicity of chemo drug and to improve therapeutic effectiveness using *in vitro* and *in vivo* model system.

Materials and Methods

Materials

Paclitaxel (PTX) was purchased from LC Laboratories (Boston, MA, USA). NuBCP-9 was custom synthesized from Bioconcept Pvt. Ltd., Maneser, Haryana. 1-Ethyl-3-(-3-diethy-laminopropyl) carbodimide (EDC) and N-hydroxysuccinamide (NHS), XTT cell proliferation kit was purchased from Cayman, USA. All the organic solvents used in the protocols are from Merck, India. Dulbecco’s modified Eagle’s medium (DMEM), fetal

bovine serum (FBS), and penicillin–streptomycin antibiotic solution were obtained from Gibco by Life Technologies, USA. Amicon ultracentrifugal filters (30 kDa) were obtained from Merck Millipore (Billerica, MA, U.S.A.). Annexin V-FITC assay kit was obtained from BD Biosciences (San Jose, U.S.A.). Ultrapure water (18 MΩ cm resistivity) was obtained from Milli-Q system (Merck Millipore, Billerica, MA, U.S.A.).

Methods

Synthesis and characterization of PLA-PEG-PPG-PEG copolymers—The biodegradable PLA-PEG-PPG-PEG tetrablock copolymer was synthesized with 72-kDa PLA (Nature Works, USA) and 12.5 kDa Poloxamer-F127 (PEG-PPG-PEG; Sigma-Aldrich, USA) by the Steglich esterification method using N-dicyclohexylcarbodimide (DCC) and 4-dimethylaminopyridine (DMAP) for conjugation as described earlier. Coupling of PLA with PEG-PPG-PEG was confirmed by GPC (Viscotek by Malvern, UK) and ^{1}HNMR (300 MHz, Brukers, U.S.A.).

Preparation and characterization of PTX and NuBCP-9 loaded nanoparticles—Loading of PTX and NuBCP-9 (Bioconcept, Gurgaon, India) into PLA-PEG-PPG-PEG NPs was performed using a double emulsion solvent evaporation method as reported by previous worker. Briefly, 10 mg of PTX was dissolved in 100 ml acetonitrile (ACN) and slowly added to 100 mg of PLA-PEG-PPG-PEG copolymer solution in 5 ml acetonitrile (ACN) in a glass vial. The resulting mixture was then added to a 20 ml aqueous phase containing 100 mg of F127 emulsifier and stirred at room temperature for 6–8 h to facilitate solvent evaporation and nanoparticle stabilization. PTX and NuBCP-9-loaded PLA-PEG-PPG-PEG NPs were also prepared by the double emulsion process. Using this approach, PTX was first added to PLA-PEG-PPG-PEG copolymer in ACN, followed by immediate addition of NuBCP-9 in the presence of slight sonication. This mixture was then added to a 20 ml aqueous phase containing F127 emulsifier and stirred at room temperature to prepare PTX-NuBCP-9/NPs. Hydrophilic Rhodamine (RhoB; Sigma Aldrich, US) and hydrophobic Coumarin-6 (Sigma Aldrich, US) dye-loaded NPs were also prepared using a similar procedure. NPs were filtered through an Amicon 30-kDa ultracentrifuge filter and washed twice with MQ water to remove free drug/dye. These washed NPs were lyophilized and stored at −20 °C until use. The filtrate was collected and analyzed for free NuBCP-9 using a Micro-BCA Kit (Pierce Biotechnology, Rockford, IL, USA) and an EPOCH microplate reader (BioTek, USA) at 590 nm. Free PTX was measured using high performance liquid chromatography (HPLC; Perkin Elmer, USA) equipped with a C18 column (250 × 4·6 mm, 5 μ) as stationary phase using mixture of acetonitrile, water and methanol (60:35:5 volume ratio) as mobile phase with a flow rate of 0.8 ml/min at a detection wavelength of 230 nm. Encapsulation efficiency (EE %) of NuBCP-9/PTX was determined using the following formula:

$$\%\,EE = \left[(PTX/NuBCP-9)_{total} - (PTX/NuBCP-9)_{filtrate}\right]/(PTX/NuBCP-9)_{total} \times 100\,.$$

Morphology and particle size of drug loaded NPs were determined using scanning electron microscopy (SEM, Zeiss EVO 50 Series) and transmission electron microscopy (TEM,

Philips Model CM12). Zeta potential of the NPs was assessed by nanoparticle tracking analysis (Nanosight, NS500, UK).

Assessment of PTX and NuBCP-9 release from NPs—*In vitro* release kinetics of PTX and NuBCP-9 from NPs were determined by an ultrafiltration method. Briefly, samples of freeze-dried drug-loaded NPs (10 mg) were suspended in PBS at pH 7.4 and incubated at 37 °C with constant shaking at 150 rpm. At predetermined time points of up to 60 days, samples were collected and ultra-filtered through 30-kDa Amicon filters (Millipore Corporation, Billerica, MA, USA). The filtrates were collected for analysis and fresh buffer was added to the respective tubes. The filtrates were analyzed for (i) PTX by HPLC, and (ii) NuBCP-9 by the micro-BCA assay.

Assessment of NP uptake—MCF-7 cells were seeded on coverslips, grown for 24 h and then incubated with RhoB and coumarin-6 loaded NPs. The coverslip was removed, washed with PBS, and the cells fixed with 4% paraformaldehyde. The cells were then stained with 4,6-diamidino-2-phenylindole (DAPI) (Invitrogen, USA) and visualized under a confocal laser scanning microscope (CLSM; Olympus, Fluoview FV1000, Japan). The cellular uptake of nanoparticles was also investigated by flow cytometry (FACS-can, Becton Dickinson, USA).

Evaluation of in vitro activity—*In vitro* cytotoxicity of the NPs was assessed in studies of human luminal hormone-dependent MCF-7 and triple-negative MDA-MB-231 breast cancer cell lines (ATCC). Cells were grown in DMEM containing 10% FBS, 100 units/mL penicillin, and 100 g/mL streptomycin (GIBCO, Life Technologies, US) in an atmosphere of 5% CO_2 at 37 °C. Exponentially growing cells were plated onto a 96-well plate at a density of 3000 cells/well and incubated for different time intervals. Free PTX in DMSO (Sigma Aldrich, USA), PTX/NPs, NuBCP-9/NPs or PTX-NuBCP-9/NPs (molar concentration of PTX /NuBCP-9 loaded in NP is calculated based on the encapsulation efficiency of PTX in the NPs and its molecular weight) were added to the wells at final drug concentrations of 0.001, 0.01, 0.1, 1, 5, 10 and 20 M. DMSO was <0.1% after dilution with cell culture medium. Tumor cell growth inhibition was evaluated using the XTT-based *in vitro* cell proliferation assay kit. The half-maximal inhibitory drug concentration (IC_{50}) was determined by the median effect equation using Graph Pad Prism software. The data are presented as mean ± SD (n = 3).

Combination index (CI) analysis—CI analysis based on the Chou and Talalay[24] method was performed using Compusyn software (version 1.0, Compusyn Inc., U.S.) to determine synergistic (CI < 1), additive (CI = 1) or antagonistic (CI > 1) cytotoxic effects of NuBCP-9 and PTX. At constant drug combination ratios, fa (fractional affect) versus CI plots was generated with Graph Pad Prism software (Version 5.0, USA).

Assessment of apoptosis caused by PTX-NuBCP-9/NPs—Cells were stained using the Annexin V-Alexa Fluor 488/PI apoptosis assay kit (Invitrogen, Molecular Probes, US). Quantification of apoptosis was performed by FACS (FACScan, Becton Dickinson, USA). The cells were also imaged using a CLSM confocal microscope.

Immunoblot analysis—Cell lysates were prepared with M-PER reagent (Pierce Chemicals, USA) and analyzed by immunoblotting with anti-Pgp1, anti-BCL-2, anti-caspase-3 cleaved fragment (CF) (Biosepses, China), anti-PARP-CF (Biosepses, China) and anti-β-actin (Santa Cruz Biotechnology, USA). Quantification of immunoblots was performed on Image J software.

In vivo antitumor efficacy—All animal experiments were approved by Institutional Animal Ethics Committee (IAEC). The study protocol approval number was 10/GO/abc/99/CPCSEA, AIIMS New Delhi, India. Mouse Ehrlich breast cancer cells were injected subcutaneously in the flank region of syngeneic BALB/c mice (17–22 g). Tumor bearing mice (~150 mm^3) were randomized into 4 groups based on body weight (6 mice/group) and treated intraperitoneally (i.p.) with 10 mg/kg of the different nanoformulations biweekly for 3 weeks. Tumors were measured by Vernier Caliper and volumes were calculated using the formula $(A \times B^2) \times 0.5$, where A and B are the longest and shortest tumor diameters, respectively. From each group, one mouse was sacrificed on day 21 for harvesting of tumor for histopathological examination. The tumors were fixed in 10% formal saline and embedded in paraffin. Five-micronsections were prepared and stained with hematoxylin and eosin (Biolab Diagnostic India Pvt. Ltd., India). Survivals of the mice were recorded till day 60 and Kaplan–Meier survival curve was prepared using Graph Pad prism 5.0 (Graph Pad Software, Dan Diego, USA) and log rank analysis was done.

Statistical analysis—All results are reported as mean ± SD and the difference between the untreated control and treated groups was evaluated statistically using the student's *t*-test. Statistical analysis of tumor volumes was performed by one-way ANOVA using Graph Pad prism 5.0 software. Sample size of at least 3 determinations was used for the analysis. Results were considered statistically significant at the level of $p < 0.05$.

Results

Drug encapsulation efficiency and in vitro release

The anti-cancer agents PTX/NuBCP-9 (single or dual) loaded biodegradable polymeric nanoparticles were prepared by double emulsion-solvent evaporation technique. Morphology and particle size of drug loaded NPs were determined using scanning electron microscopy and transmission electron microscopy (Figure 1). Drug loaded nanoparticles showed smooth and spherical morphology with the size range of 100–120 nm as per SEM and TEM, respectively.

The encapsulation efficiency of PTX and NuBCP-9 in tetrablock PLA–PEG-PPG-PEG NPs are presented in Table 1. The PLA–PEG-PPG-PEG copolymer is hydrophobic due to its high PLA content (84%). In concert with this relative hydrophobicity, we achieved 88% encapsulation of hydrophobic PTX, as compared to 65% encapsulation of the hydrophilic NuBCP-9 (Table 1). Different ratios of PTX and NuBCP-9 were then encapsulated into the NPs to assess the effects of dual loading. The encapsulation efficiency of PTX was found to be >90% in all of the PTX-NuBCP-9 encapsulated nanoformulations. By contrast, increased levels of NuBCP-9 encapsulation were achieved at PTX:NuBCP-9 ratios of 1:1 and 1:3, as compared to that at 3:1 (Table 1). DLS measurements of empty NPs were in the range of 104

nm, which increased to 130 nm and 165 nm with loading of PTX and PTX-NuBCP-9, respectively (Table 1). Likewise, there was no significant increase in particle size in serum containing DMEM (Table S1), thus indicating the stability of nanoparticles. Zeta potentials of the NPs were more negative with increases in NuBCP-9 encapsulation (Table 1); conceivably because interactions of the positively charged NuBCP-9 with the negatively charged PLA which results in increase in number of peptide carboxyl groups on the surface of nanoparticles. PTX is loaded in the hydrophobic core of PLA while peptide is encapsulated in the outer hydrophilic shell of the PLA–PEG-PPG-PEG copolymeric nanoparticles.

The *in vitro* release profiles of PTX and NuBCP-9 from the NPs was evaluated at physiological pH. Cumulative release of PTX from PTX/NPs was ~47% over 7 days (Figure 2, *A*, left). At initial days, the spurt percentage release/day of encapsulated PTX was ~10% followed by sustained release of ~1–3% was observed till 60 days of the study period (Figure 2, *A*, right). Percentage cumulative release (Figure 2, *B*, left) and percentage release/day (Figure 2, *B*, right) of NuBCP-9 from NuBCP-9/NPs was comparable to that obtained for the PTX/NPs. Importantly, the co-release of PTX and NuBCP-9 from PTX-NuBCP-9/NPs was 30% and 40%, respectively, over 10 days (Figure 2, *C*, left). In addition, release over 60 days of PTX and NuBCP-9 was ~60% and ~70%, respectively, from the PTX-NuBCP-9/NPs (Figure 2, *C*, left). Moreover, percentage release/day of PTX from the PTX-NuBCP-9/NPs was similar to that for PTX/NPs (Figure 2, *C*, right). In contrast, percentage release/day for NuBCP-9 from PTX-NuBCP-9/NPs was slightly delayed compared to that for NuBCP-9/NPs. These findings demonstrated that (i) encapsulation of both PTX and NuBCP-9 is achievable in the same NPs and (ii) release of PTX and NuBCP-9 is sustained from PTX-NuBCP-9/NPs.

Effects of PTX and NuBCP-9 NP formulations on intracellular drug uptake and survival

Confocal imaging and FACS studies of hydrophilic RhoB-or hydrophobic Coumarin-6-loaded polymeric NPs confirmed the intracellular uptake of both dyes throughout the cytosol (Figure 3, *A*). Further, we investigated the intracellular localization of NuBCP-9 when treating MCF-7 cells with FITC-NuBCP-9 encapsulated in our tetra block PLA–PEG-PPG-PEG NPs. FITC-NuBCP-9 localized to the cytoplasm and mitochondria as evidenced by staining with Mitotracker (Figure 3, *B*, upper panel). The intensity of binding was calculated using the image analysis software which showed a Pearson's coefficient (PC) of 0.95%, indicating the strong affinity of binding NuBCP-9 at BCL-2 proteins present on mitochondria. In agreement with those and the above studies, confocal analysis of MCF-7 cells treated with FITC-PTX/NPs and RhoB-NuBCP-9/ NPs demonstrated the colocalization of PTX and NuBCP-9 in the cytosol and mitochondria (Figure 3, *B*, lower panel). The pearson coefficient of 0.49% clearly demonstrates the partial co-localization or negligible competitiveness among both the targets. This study clearly demonstrated that PTX preferably bound to microtubules in cytosol while NuBCP-9 specifically acted on BCL-2 protein in the mitochondria.

To investigate effects of the NPs on survival, MCF-7 cells were exposed to NPs encapsulated with different ratios of PTX: NuBCP-9 (3:1, 1:1 and 1:3). Significant inhibition of MCF-7

cell growth was observed with the different nanoformulations (Figure 4, *A*). Moreover, treatment with NPs encapsulated with PTX:NuBCP-9 at a 1:1 ratio was associated with maximum growth inhibition (Figure 4, *A*). Similar results were obtained when treating MDA-MB-231 cells (Figure 4, *B*). Based on these findings, subsequent studies were performed with NPs containing PTX:NuBCP-9 at the 1:1 ratio. To determine whether PTX-NuBCP-9/NPs were more effective than physical mixture of PTX/NPs with NuBCP-9/NPs, we first determined the half-maximal growth inhibitory concentrations (IC_{50}s) for PTX/NPs and NuBCP-9/NPs. In studies with MCF-7 cells, the IC_{50}s for PTX/NPs and NuBCP-9/NPs were 43 nM and 2 μM, respectively (Figure 4, *C*, left; Table 2). Additionally, the IC_{50} values for PTX/NPs and NuBCP-9/NPs in combination was decreased to 17 nM and PTX-NuBCP-9/NPs showed 1 nM (Figure 4, *C*, right; Table 2). Comparable results were obtained for MDA-MB-231 cells (Figure 4, *D*, left and right; Table 2), indicating strong activity with PTX-NuBCP-9/NPs as compared treatment with PTX/NPs or NuBCP-9/NPs alone. Although, free PTX and NuBCP-9[23] showed comparable to drug loaded in tetrablock coplymeric NPs. Thus, acting as control for dual PTX-NuBCP loaded NPs.

Combination effects of PTX-NuBCP-9/NPs against breast carcinoma cells

To find out the combination effects, 10 nM of each NPs such as PTX/NPs, NuBCP-9/NPs, PTX-NuBCP-9/NPs, physical mixture of PTX/NPs and NuBCP-9/NPs were used to treat MCF-7 cells. The results demonstrated synergistic inhibition of MCF-7 cell viability in response to treatment with PTX-NuBCP-9/NPs (Figure 5, *A*). Similar effects of PTX-NuBCP-9/NPs were obtained in studies of MDA-MB-231 cells (Figure 5, *B*). As a control, empty NPs had little, if any, effect on viability, supporting their biocompatibility and lack of toxicity. To further substantiate these findings, MCF-7 cells were treated with different concentrations of PTX/NPs, NuBCP-9/NPs or PTX-NuBCP-9/NPs. CI analysis was done by Chou and Talalay method using Compusyn software.[24] The results demonstrated synergy with CI values <0.2 (Figure 5, *C*). Similar results were obtained with MDA-MB-231 cells (Figure 5, *D*), indicating that PTX-NuBCP-9/NPs were synergistic in inhibiting growth and survival of breast carcinoma cells.

Assessment of apoptosis caused by PTX-NuBCP-9/NPs

To assess effects on induction of apoptosis, MCF-7 cells treated with the NP formulations were monitored by Annexin V/ PI staining. Confocal images demonstrated that treatment with PTX-NuBCP-9/NPs results in greater Annexin-V staining than PTX/NPs or NuBCP-9/NPs alone, consistent with the induction of an enhanced apoptotic response (Figure 6, *A*). Quantification of Annexin V/PI staining by FACS confirmed that PTX-NuBCP-9/NPs were significantly more effective than PTX/NPs or NuBCP-9/NPs in inducing apoptosis (Figure 6, *B*, Table S2). NuBCP-9 targeted mitochondrial BCL-2 and thereby induced apoptosis.[21] Interestingly, we found that treatment of MCF-7 cells with PTX-NuBCP-9/NPs was associated with significant downregulation of BCL-2 levels, a response more pronounced than that obtained with PTX/NPs or NuBCP-9/NPs as confirmed by immunoblot analysis (Figure 6, *C*). In concert with these results, we also found that PTX-NuBCP-9/NPs were more effective than PTX/NPs or NuBCP-9/NPs in activation of the intrinsic apoptotic pathway as evidenced by caspase-3 cleavage (Figure 6, *C*). These findings

supported the hypothesis that PTX-NuBCP-9/NPs were more active in inducing apoptosis of MCF-7 cells than PTX/NPs or NuBCP-9/NPs.

In vivo antitumor efficacy of PTX-NuBCP-9/NPs

Before initiating *in vivo* studies different concentrations of polymeric NPs were tested for hemolysis and it was found that the PLA–PEG-PPG-PEG nanoparticles showed no significant blood hemotoxicity and hence the developed biodegradable polymeric nanoparticles are biocompatible (Figure S1). To investigate whether PTX-NuBCP-9/NPs are effective in inhibiting tumor growth, we performed studies in BALB/c mice bearing established subcutaneous Ehrlich breast cancer tumors. Based on the kinetics of PTX and NuBCP-9 release from NPs over 7 days (Figure 2), we treated Ehrlich tumor-bearing mice i.p. twice a week for 3 weeks. As compared with mice treated with empty NPs, treatment with 10 mg/kg PTX/NPs was associated with partial regression of the tumors (Figure 7, *A*). However, treatment with 10 mg/kg PTX-NuBCP-9/NPs was associated with significant and prolonged tumor regressions (Figure 7, *A*). Analysis of survival as determined by Kaplan–Meier plots further demonstrated that mice treated with PTX-NuBCP-9/NPs survived significantly longer ($p = 0.0135$, Log rank analysis) than those treated with empty NPs, PTX/NPs or NuBCP-9/NPs (Figure 7, *B*). In addition, there was no weight loss or other overt toxicities observed in mice treated with PTX-NuBCP-9/NPs. Tumors harvested from mice treated with empty NPs on day 21 exhibited little, if any, evidence of necrosis (Figure 7, *C*). By contrast, tumor cells from PTX/NP-treated and NuBCP-9/NP-treated mice exhibited necrosis, as evidenced by pyknotic nuclei and loss of morphology (Figure 7, *C*). However, mice treated with PTX-NuBCP-9/NPs had no detectable Ehrlich tumor cells, consistent with the observed significant tumor regressions (Figure 7, *C*).

Activity of PTX-NuBCP-9/NPs against MCF-7 cells resistant to PTX (MCF-7/PTX-R)

The above findings supported the concept that the PTX-NuBCP-9/NPs might be effective against PTX-resistant cells. To investigate this possibility, we did some preliminary studies on MCF-7 cells resistant to PTX. The resistance in MCF-7 cells was confirmed by immunocytochemistry (Figure 8, *A*). Over expression of BCL-2 and generation of Pgp1 proteins confirmed the resistance in MCF-7 cells (Figure 8, *A*).We treated MCF-7/PTX-R cells with PTX-NuBCP-9/NPs and found an IC_{50} of 10.3 nM, which was ~64-fold lower than that obtained with PTX alone (Table 3). Additionally, treatment of MCF-7/PTX-R cells with PTX-NuBCP-9/NPs was associated with marked down regulation BCL-2 and Pgpl levels (Figure 8, *B*). These findings proved that PTX-NuBCP-9/NPs targeted BCL-2 effectively and worked against PTX resistant MCF-7 cells.

Discussion

PTX was initially developed for breast cancer treatment in a solvent-based formulation consisting of polyoxyethylated castor oil, which was associated with clinically significant hypersensitivity reactions. *Nab*-paclitaxel (Abraxane) is a second generation formulation in which PTX is encapsulated in solvent-free albumin NPs.[25] *Nab*-paclitaxel can be delivered at higher doses than PTX, in part, by limiting the hypersensitivity reactions.[26] In addition, *nab*-paclitaxel was found to be more effective than PTX in the treatment of patients with

breast cancer.[26–28] Thus, the approval of *nab*-paclitaxel for the treatment of breast, as well as NSCLC and pancreatic, cancers has supported the effectiveness of delivering PTX in a NP formulation. However, the progression-free survival for PTX and *nab*-paclitaxel as first-line treatment of locally recurrent or metastatic breast cancer is 11 and 9.3 months, respectively[29] emphasizing the need for more effective therapies that circumvent the development of resistance. The present studies demonstrated the feasibility of encapsulating PTX into polymeric tetra-block NPs, which were developed for the sustained intracellular delivery of other anti-cancer agents.[23,30] Our results demonstrated that PTX/NPs were active against breast cancer cells and, importantly, are highly potent in the setting of PTX resistance.

PTX-induced resistance has been associated with alterations in the mitochondrial apoptotic pathway, including the upregulation of BCL-2 and BCL-xL.[31–35] One approach to reversing this mechanism of PTX resistance has been by combining PTX with navitoclax (ABT-263), a small molecule inhibitor of BCL-2, BCL-xL and BCL-w.[31,32] However, this strategy is likely to have limited effects clinically in that PTX efflux from multi-drug resistant (MDR) cells would remain as an overarching obstacle.[34,35] The present studies have thus explored the potential of including NuBCP-9 in the PTX/NPs as a way of blocking PTX efflux and inhibiting BCL-2. NuBCP-9 binds to BCL-2 and induces a conformational change that neutralizes BCL-2-mediated inhibition of BAX.[21] In addition, binding of NuBCP-9 to BCL-2 exposes the BCL-2 BH3 domain and inhibits BCL-xL.[21] Importantly, NuBCP-9 thus induces apoptosis of cancer, but not normal, cells.[21] Based on these findings and previous work, we showed that encapsulation of NuBCP-9 in our polymeric NPs was an effective approach for the sustained delivery of NuBCP-9 and those NuBCP-9/NPs were active against breast cancer cells growing *in vitro* as well as in mice.[23] In previous studies, it was demonstrated that the *in vitro* internalization of PLA-based NPs was through endocytosis[36–38] and was associated with surface charge reversal (anionic to cationic) in the acidic pH of the endo-lysosomes. This charge reversal facilitated interaction of the NPs with vesicular membranes, leading to transient and localized membrane destabilization, and thereby escaped of the NPs into the cytosol.[23] Nanoparticles also have the tendency to go inside the fastest dividing cells in the body by the enhanced permeability and retention (EPR) effect. Since tumor cells are the fastest dividing cells, the uptake of NPs is significantly more in these cells.[39] Photoaffinity cross linking studies reported the localization of PTX binding to tubulin in microtubules[40,41] and in mitochondria.[42] However, our confocal studies clearly demonstrated that PTX preferably bound to microtubules in cytosol while NuBCP-9 specifically targeted BCL-2 protein in the mitochondria. Our present results further demonstrated that both PTX and NuBCP-9 can be encapsulated in the same NPs, providing an approach to target BCL-2/BCL-xL. PTX is also shown to down regulate BCL-2 expression. Thus results of the present studies have shown complete down regulation of BCL-2 expression with both PTX and NuBCP-9. Indeed, treatment of PTX-resistant MCF-7 cells with PTX-NuBCP-9/ NPs was ~64 fold more effective than PTX, supporting the contribution of NuBCP-9 to the combination. This might be due to the role of pluronics in inhibiting the Pgp1 receptors[20] which got released due to the biodegradation of PLA–PEG-PPG-PEG NPs in the acidic environment of the cancer cells.

Previous studies with tetra-block PLA–PEG-PPG-PEG NPs have shown that their systemic administration for the sustained delivery of NuBCP-9 and other anti-cancer peptides was active in mouse tumor models and associated with little if any toxicity.[23,30] In the present work, treatment of Ehrlich breast tumor-bearing mice with PTX-NuBCP-9/NPs was more effective than that obtained with PTX/NPs or NuBCP-9/NPs alone. Moreover, the developed nanoparticles with slight negative surface charge have been shown to be most effective in achieving enhanced tumor accumulation and prolonged circulation.[43–45] In addition, these NP formulations were well tolerated. In this regard, polymeric PLA–PEG NPs have shown to be nontoxic and biodegradable and are undergoing clinical evaluation.[46–48] For example, Genexol-PM is a PTX-loaded PLA–PEG micelle formulation that is undergoing Phase II evaluation for the treatment of metastatic cancers.[46,49] Moreover, BIND-014 is a docetaxel-encapsulated PLA–PEG NP that is targeted to prostate-specific antigen.[50] Encapsulation of AZD2811, an Aurora B kinase inhibitor, in PLA–PEG NPs has further demonstrated improved efficacy and tolerability in preclinical models.[51] These findings and the present demonstration that PTX-NuBCP-9/NPs are effective against paclitaxel-resistant breast cancer cells support further development of these novel PLA–PEG-PPG-PEG NPs for the treatment of advanced breast and other cancers. The results of the present study described a novel, safe and effective nanoformulation for treating MDR cancer using novel polymeric nanoformulation that targets cellular mechanism as well as controlled delivery of the drug at the specific site.

In conclusion, combination of PTX and the BCL-2 inhibitor, NuBCP-9 loaded PTX-NuBCP-9/NPs was synergistic against breast cancer cells in *in vitro* and in syngenic BALB/c mice model. In addition, PLA–PEG-PPG-PEG based nanoparticles have the potential both as Pgp1 inhibitor and as nanocarriers for small molecule inhibitors and anticancer peptides. Our results demonstrated that PTX-NuBCP-9/NPs loaded PLA–PEG-PPG-PEG nanoparticles has strong potential as nanomedicine for cancer therapy, however, additional *in vivo* work is warranted.

Supplementary Material

Refer to Web version on PubMed Central for supplementary material.

Acknowledgments

Financial support: Research reported in this publication was funded by Department of Science and Technology, Government of India (SR/NM/NS-1091/2015) and also supported by National Cancer Institute of National Institutes of Health, USA under award number CA97098 and CA166480.

Abbreviations

NP	nanoparticle
P-gp	Poly-glycoproteins
PTX	Paclitaxel
nab-paclitaxel	albumin based paclitaxel loaded nanoparticles

NuBCP-9	Nur77 derived BCL-2 converting 9 mer peptide
caspase-3-CF	caspase-3-cleaved fragment
EAT	Ehrlich ascites tumor
IP	intraperitoneal
PDI	polydispersity index
TEM	transmission electron microscopy
SEM	scanning electron microscopy
CLSM	confocal laser scanning microscopy

References

1. Holmes FA, Walters RS, Theriault RL, Forman AD, Newton LK, Raber MN, et al. Phase II trial of taxol, an active drug in the treatment of metastatic breast cancer. J Natl Cancer Inst. 1991; 83:1797–805. [PubMed: 1683908]
2. Brown T, Havlin K, Weiss G, Cagnola J, Koeller J, Kuhn J, et al. A phase I trial of taxol given by a 6-hour intravenous infusion. J Clin Oncol. 1991; 9:1261–7. [PubMed: 1675263]
3. Mc Guire WP, Rowinsky EK, Rosenshein NB, Grumbine FC, Ettinger DS, Armstrong DK, et al. Taxol: a unique antineoplastic agent with significant activity in advanced ovarian epithelial neoplasms. Ann Intern Med. 1989; 111:273–9. [PubMed: 2569287]
4. Jordan MA, Kamath K. How do microtubule-targeted drugs work? An overview. Curr Cancer Drug Targets. 2007; 7:730–42. [PubMed: 18220533]
5. Fuchs DA, Johnson RK. Cytologic evidence that taxol, an antineoplastic agent from Taxusbrevifolia, acts as a mitotic spindle poison. Cancer Treat Rep. 1978; 62:1219–22. [PubMed: 688258]
6. Schiff PB, Horwitz SB. Taxol stabilizes microtubules in mouse fibroblast cells. S A. 1980; 77:1561–5.
7. Schiff PB, Horwitz SB. Taxol assembles tubulin in the absence of exogenous guanosine 5′-triphosphate or microtubule-associated proteins. Biochemistry. 1981; 20:3247–52. [PubMed: 6113842]
8. Schiff PB, Fant J, Horwitz SB. Promotion of microtubule assembly in vitro by taxol. Nature. 1979; 277:665–7. [PubMed: 423966]
9. Haldar S, Jena N, Croce CM. Proc Natl Acad Sci USA. 1995; 92:4507–11. [PubMed: 7753834]
10. Kundranda MN, Niu J. Albumin-bound paclitaxel in solid tumors: clinical development and future directions. Drug Des Devel Ther. 2015; 9:3767–77.
11. Wiernik PH, Schwartz EL, Strauman JJ, Dutcher JP, Lipton RB, Paietta E. Phase I clinical and pharmacokinetic study of taxol. Cancer Res. 1987; 47:2486–93. [PubMed: 2882837]
12. Wiernik PH, Schwartz EL, Einzig A, Strauman JJ, Lipton RB, Dutcher JP. Phase-I trial of taxol given as a 24-hour infusion every 21 days: responses observed in metastatic melanoma. J Clin Oncol. 1987; 5:1232–9. [PubMed: 2887641]
13. Zhao MD, Hu FQ, Du YZ, Yuan H, Chen FY, Lou YM, et al. Co-administration of glycolipid-like micelles loading cytotoxic drug with different action site for efficient cancer chemotherapy. Nanotechnology. 2009; 20
14. Shin HC, Alani AW, Rao DA, Rockich NC, Kwon GS. Multi-drug loaded polymeric micelles for simultaneous delivery of poorly soluble anticancer drugs. J Control Release. 2009; 140:294–300. [PubMed: 19409432]
15. Wang Y, Gao S, Ye WH, Yoon HS, Yang YY. Co-delivery of drugs and DNA from cationic core-shell nanoparticles self-assembled from a biodegradable copolymer. Nat Mater. 2006; 5:791–6. [PubMed: 16998471]

16. Wang S, Ren W, Liu J, Lahat G, Torres K, Lopez G, et al. TRAIL and doxorubicin combination induces proapoptotic and antiangiogenic effects in soft tissue sarcoma in vivo. Clin Cancer Res. 2010; 16:2591–604. [PubMed: 20406839]
17. Hossain MA, Kim DH, Jang JY, Kang YJ, Yoon JH, Moon JO, et al. Aspirin enhances doxorubicin-induced apoptosis and reduces tumor growth in human hepatocellular carcinoma cells in vitro and in vivo. Oncol. 2012; 40:1636–42.
18. Jin C, Li H, He Y, He M, Bai L, Cao Y, et al. Combination chemotherapy of doxorubicin and paclitaxel for hepatocellular carcinoma in vitro and in vivo. J Cancer Res Clin Oncol. 2010; 136:267–74. [PubMed: 19693537]
19. Hunter R, Olsen M, Buynitzky S. Adjuvant activity of non-ionic block copolymers IV. Effect of molecular weightand formulation on titre and isotype of antibody. Vaccine. 1991; 9:250–6. [PubMed: 2058267]
20. Kabanova AV, Batrakovaa EV, Alakhovb VY. Pluronic® block copolymers for overcoming drug resistance in cancer. Adv Drug Deliv Rev. 2002; 54:759–79. [PubMed: 12204601]
21. Kolluri SK, Zhu X, Zhou X, Lin B, Chen Y, Sun K, et al. A short Nur77-derived peptide converts Bcl-2 from a protector to a killer. Cancer Cell. 2008; 14:285–98. [PubMed: 18835031]
22. Watkins CL, Sayers EJ, Allender C, Barrow D, Fegan C, Brennan P, et al. Co-operative membrane disruption between cell-penetrating peptide and cargo: implications for the therapeutic use of the Bcl-2 converter peptide D-NuBCP-9-r8. Mol Ther. 2011; 19:2124–32. [PubMed: 21934653]
23. Kumar M, Gupta D, Singh G, Sharma S, Bhatt M, Prashant CK, et al. Novel polymeric nanoparticles for intracellular delivery of peptide cargos: antitumor efficacy of the BCL-2 conversion peptide NuBCP-9. Cancer Res. 2014; 74:3271–81. [PubMed: 24741005]
24. Chou TC. Drug combination studies and their synergy quantification using the Chou-Talalay method. Cancer Res. 2010; 70:440–6. [PubMed: 20068163]
25. Ibrahim NK, Samuels B, Page R, Doval D, Patel KM, Rao SC, et al. Multicenter phase II trial of ABI-007, an albumin-bound paclitaxel, in women with metastatic breast cancer. J Clin Oncol. 2005; 23:6019–26. [PubMed: 16135470]
26. Gradishar WJ, Tjulandin S, Davidson N, Shaw H, Desai N, Bhar P, et al. Phase III trial of nanoparticle albumin-bound paclitaxel compared with polyethylated castor oil-based paclitaxel in women with breast cancer. J Clin Oncol. 2005; 23:7794–803. [PubMed: 16172456]
27. Blum JL, Savin MA, Edelman G, Pippen JE, Robert NJ, Geister BV, et al. Phase II study of weekly albumin-bound paclitaxel for patients with metastatic breast cancer heavily pre-treated with taxanes. Clin Breast Cancer. 2007; 7:850–6. [PubMed: 18269774]
28. Gradishar WJ, Krasnojon D, Cheporov S, Makhson AN, Manikhas GM, Clawson A, et al. Phase II trial of nab-paclitaxel compared with docetaxel as first-line chemotherapy in patients with metastatic breast cancer: final analysis of overall survival. Clin Breast Cancer. 2012; 12:313–21. [PubMed: 22728026]
29. Rugo HS, Barry WT, Moreno-Aspitia A, Lyss AP, Cirrincione C, Leung E, et al. Randomized phase III trial of paclitaxel once per week compared with nanoparticle albumin-bound nab-paclitaxel once per week or ixabepilone with bevacizumab as first-line chemotherapy for locally recurrent or metastatic breast cancer: CALGB 40502/NCCTG N063H (Alliance). J Clin Oncol. 2015; 33:2361–9. [PubMed: 26056183]
30. Hasegawa M, Sinha RK, Kumar M, Alam M, Yin L, Raina D, et al. Intracellular targeting of the oncogenic MUC1-C protein with a novel GO-203 nanoparticle formulation. Clin Cancer Res. 2015; 21:2338–47. [PubMed: 25712682]
31. Kutuk O, Letai A. Alteration of the mitochondrial apoptotic pathway is a key to acquired paclitaxel resistance and can be reversed by ABT-737. Cancer Res. 2008; 68:7985–94. [PubMed: 18829556]
32. Tan N, Malek M, Zha J, Yue P, Kassees R, Berry L, et al. Navitoclax enhances the efficacy of taxanes in non-small cell lung cancer models. Clin Cancer Res. 2011; 17:1394–404. [PubMed: 21220478]
33. Dai H, Ding H, Meng XW, Lee SH, Schneider PA, Kaufmann SH. Contribution of Bcl-2 phosphorylation to Bak binding and drug resistance. Cancer Res. 2013; 73:6998–7008. [PubMed: 24097825]

34. Barbuti AM, Chen ZS. Paclitaxel through the ages of anticancer therapy: Exploring Its role in chemoresistance and radiation therapy. Cancers (Basel). 2015; 7:2360–71. [PubMed: 26633515]
35. Zhao, Y; Mu, X; Du, G. Microtubule-stabilizing agents: New drug discovery and cancer therapy. Pharmacol Ther. 2015.
36. Mao Z, Zhou X, Gao C. Influence of structure and properties of colloidal biomaterials on cellumar uptake and cell functions. Biomater Sci. 2013; 1:896–911.
37. Behzadi S, Serpooshan V, Tao W, Hamaly MA, Alkawareek MY, Dreaden EC, et al. Cellular uptake of nanoparticles: journey inside the cell. Chem Soc Rev. 2017; 46:4218–44. [PubMed: 28585944]
38. Rapid endo-lysosomal escape of poly(DL-lactide-co-glycolide) nanoparticles:implications for drug and gene delivery. FASEB J. 2002; 16:1217–1226. [PubMed: 12153989]
39. Bertrand N, Grenier P, Mahmoudi M, Lima EM, Appel EA, Dormont F. Mechanistic understanding of in vivo protein corona formation on polymeric nanoparticles and impact on pharmacokinetics. Nat Commun. 2017; 8:1–8. [PubMed: 28232747]
40. Rao S, Orr GA, Chaudhary AG, Kingston DG, Horwitz SB. Characterization of the taxol binding site on the microtubule 2-(m-Azidobenzoyl) taxolphotolabels a peptide (amino acids 217–231) of beta-tubulin. J Biol Chem. 1995; 270:20235–8. [PubMed: 7657589]
41. Rao S, He L, Chakravarty S, Orr GA, Horwitz SB. Characterization of the Taxol binding site on the microtubule. Identification of Arg (282) in beta-tubulin as the site of photoincorporation of a 7-benzophenone analogue of Taxol. J Biol Chem. 1999; 274:37990–4. [PubMed: 10608867]
42. Carre M, Andre N, Carles G, Borghi H, Brichese L, Briand C, et al. Tubulin is an inherent component of mitochondrial membranes that interacts with the voltage-dependent anion channel. J Biol Chem. 2002; 277:33664–9. [PubMed: 12087096]
43. He C, Hu Y, Yin L, Tang C, Yin C. Effects of particle size and surface charge on cellular uptake and biodistribution of polymeric nanoparticles. Biomaterials. 2010; (13):3657–3666. [PubMed: 20138662]
44. Lee, SY, Cheng, JX. Clearance of nanoparticles during circulation. In: Yeo, Y, editor. Nanoparticulate Drug delivery systems: strategies, technologies, and applications. New Jersey: John Wiley & Sons, Inc; 2013. 1–324.
45. Kim ST, Saha K, Kim C, Rotello VM. The role of surface functionality in determining nanoparticle cytotoxicity. Acc Chem Res. 2013; 46:681–91. [PubMed: 23294365]
46. Kamaly N, Xiao Z, Valencia PM, Radovic-Moreno AF, Farokhzad OC. Targeted polymeric therapeutic nanoparticles: design, development and clinical translation. Chem Soc Rev. 2012; 41:2971–3010. [PubMed: 22388185]
47. Xiao RZ, Zeng ZW, Zhou GL, Wang JJ, Li FZ, Wang AM. Recent advances in PEG-PLA block copolymer nanoparticles. Nanomedicine. 2010; 5:1057–65.
48. Alexis F, Pridgen EM, Langer R, Farokhzad OC. Nanoparticle Technologies for Cancer Therapy. Handb Exp Pharmacol. 2010; 197:55–86.
49. Kim TY, Kim DW, Chung JY, Shin SG, Kim SC, Heo DS, et al. Phase I and pharmacokinetic study of Genexol-PM, a cremophor-free, polymeric micelle-formulated paclitaxel, in patients with advanced malignancies. Clin Cancer Res. 2004; 10:3708–16. [PubMed: 15173077]
50. Hrkach J, Von Hoff D, Mukkaram Ali M, Andrianova E, Auer J, Campbell T, et al. Preclinical development and clinical translation of a PSMA-targeted docetaxel nanoparticle with a differentiated pharmacological profile. Sci Transl Med. 2012; 4:128–39.
51. Ashton S, Song YH, Nolan J, Cadogan E, Murray J, Odedra R, et al. Aurora kinase inhibitor nanoparticles target tumors with favourable therapeutic index in vivo. Sci Transl Med. 2016; 8:317–25.

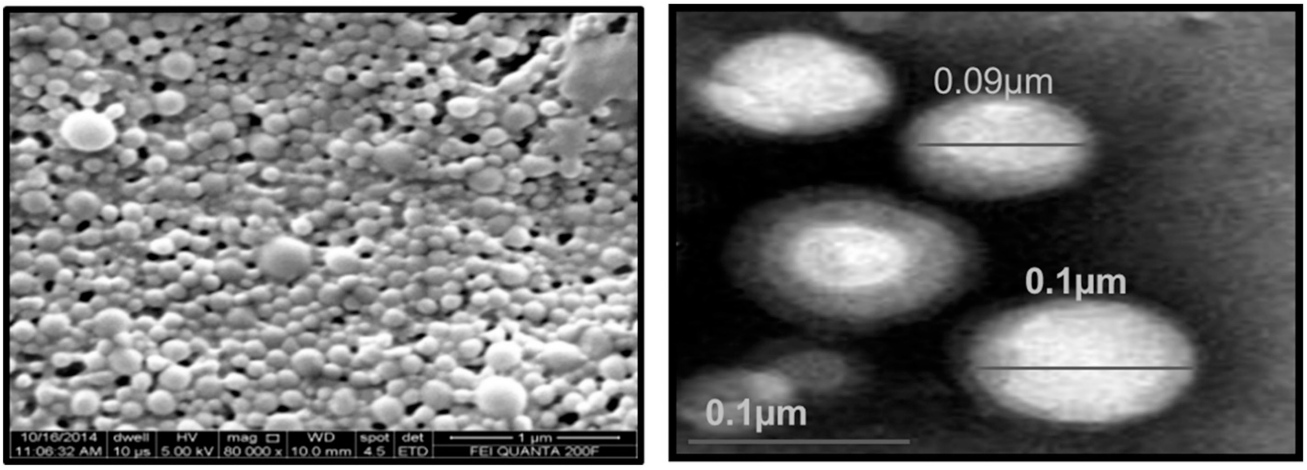

Figure 1.
SEM and TEM images of PLA–PEG-PPG-PEG tetra-block NPs.

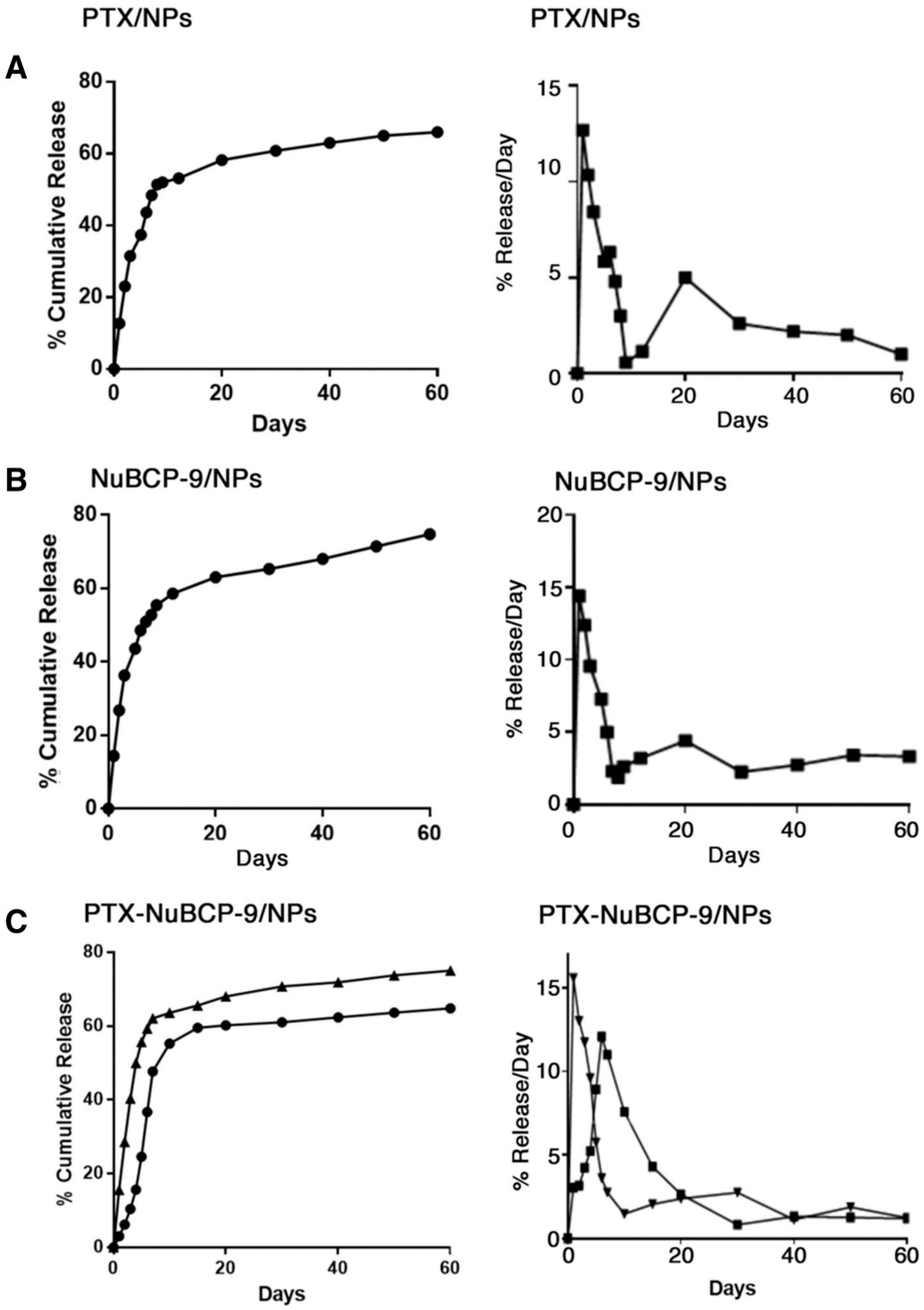

Figure 2.

Release of PTX and NuBCP-9 from NPs *in vitro*. (**A**) Left panel. Release of PTX from PTX/NPs is represented as a percentage of PTX released cumulatively each day (mean ± SD of 3 replicates) in PBS at pH 7.4. Right panel. Release of PTX from PTX/NPs is represented as a percentage of PTX release per day (mean ± SD of 3 replicates) in PBS at pH 7.4. (**B**) Left panel. Release of NuBCP-9 from NuBCP-9/NPs is represented as a percentage of NuBCP-9 released cumulatively each day (mean ± SD of 3 replicates) in PBS at pH 7.4. Right panel. Release of NuBCP-9 from NuBCP-9/NPs is represented as a percentage of NuBCP-9 release per day (mean ± SD of 3 replicates) in PBS at pH 7.4. (**C**) Left panel.

Release of PTX and NuBCP-9 from NuBCP-9/PTX/NPs is represented as a percentage of PTX (circles) and NuBCP-9 (triangles) released cumulatively each day (mean ± SD of 3 replicates) in PBS at pH 7.4. Right panel. Release of PTX and NuBCP-9 from PTX-NuBCP-9/NPs is represented as a percentage of PTX (squares) and NuBCP-9 (triangles) release per day (mean ± SD of 3 replicates) in PBS at pH 7.4.

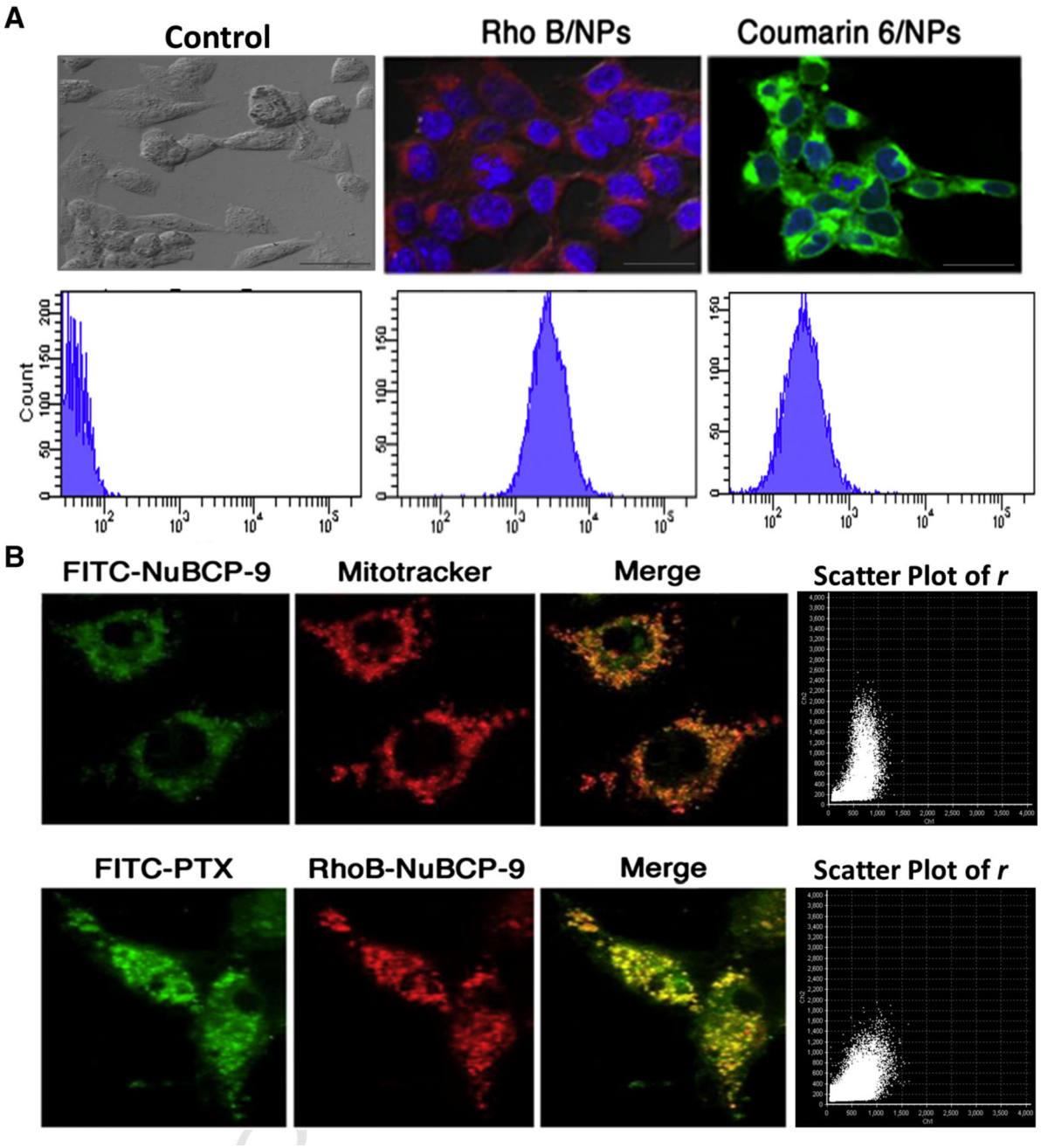

Figure 3.

Cellular uptake studies and effects of NPs on intracellular localization of PTX and NuBCP-9. (**A**) Upper panel. MCF-7 cells were treated with NPs encapsulated with the RhoB or Coumarin-6 dyes for 12 h. After washing, the cells were fixed and visualized by confocal microscopy (60X magnification). Lower panel. MCF-7 cells were treated with NPs encapsulated with the RhoB or Coumarin-6 dyes for 12 h and cellular uptake was quantified by FACS. (**B**) Upper panel. MCF-7 cells were treated with FITC-labeled NuBCP-9/NPs for 12 h. After washing, the cells were fixed and visualized by confocal microscopy (100X magnification). Mitochondria were stained with mitochondria selective Mitotracker dye.

Green signal, FITC-NuBCP-9. Red signal, Mitotracker. Yellow/ orange signal, colocalization of NuBCP-9 and Mitotracker. Scatter plot graph of Pearson's correlation coefficient (r) Lower panels. MCF-7 cells were treated with NPs encapsulated with both FITC-labeled PTX and Rho-NuBCP-9 for 12 h. After washing, the cells were fixed and visualized by confocal microscopy (100X magnification). Green signal, FITC-labeled PTX. Red signal, RhoB-labeled NuBCP-9. Yellow/orange signal, colocalization of PTX and NuBCP-9. Scatter plot graph of Pearson's correlation coefficient (r).

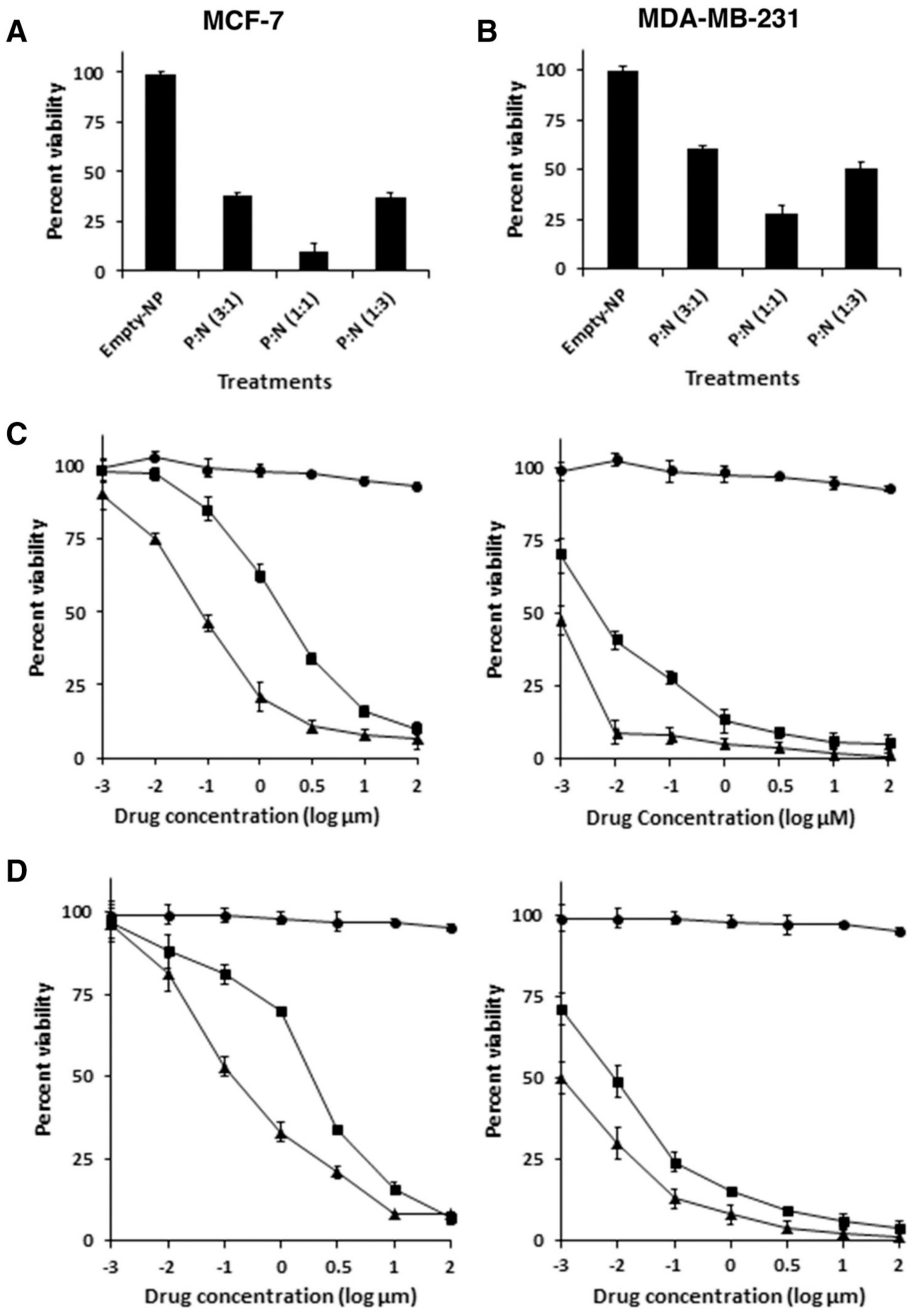

Figure 4.

Effects of NPs on intracellular localization of PTX and NuBCP-9, and cell survival. (**A** and **B**) MCF-7 (**A**) and MDA-MB-231 (**B**) cells were treated with NPs encapsulated with both PTX and NuBCP-9 at the indicated ratios. After 72 h, the cells were analyzed by XTT assays. The results are presented as percentage viability (mean ± SD of three independent experiments). (**C** and **D**) Left panels. MCF-7 (**C**) and MDA-MB-231 (**D**) cells were treated with the indicated concentrations of empty NPs (circles), PTX/NPs (triangles) or NuBCP-9/NPs (squares) for 72 h. Cell viability was determined by XTT assays. The results are presented as percentage viability (mean ± SD of three independent experiments). Right

panels. The indicated cells were treated with different concentrations of empty NPs (circles), PTX/NPs + NuBCP-9/NPs (squares) or PTX-NuBCP-9/NPs (triangles) for 72 h. Cell viability was determined by XTT assays. The results are presented as percentage viability (mean ± SD of three independent experiments).

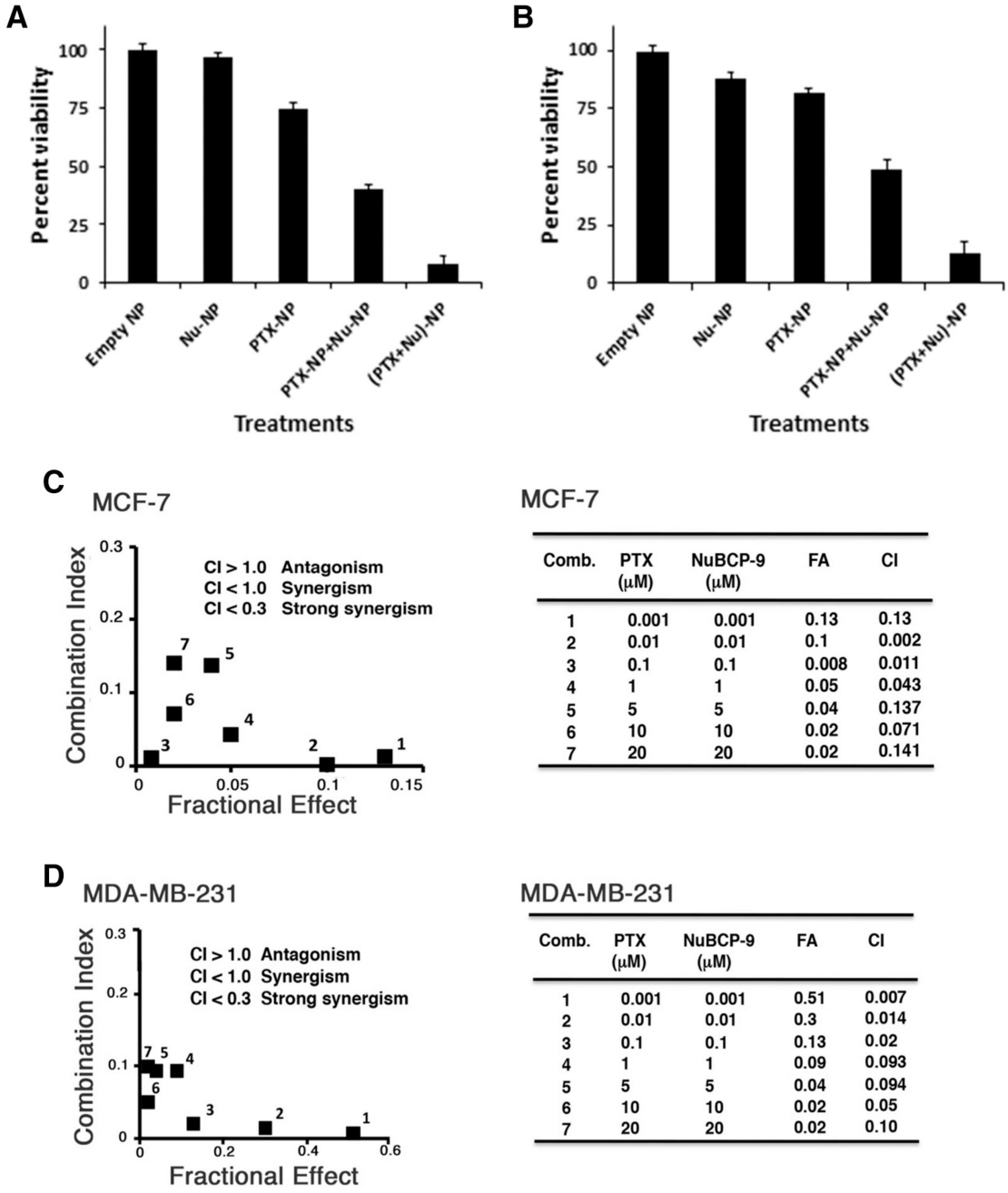

Comb.	PTX (μM)	NuBCP-9 (μM)	FA	CI
1	0.001	0.001	0.13	0.13
2	0.01	0.01	0.1	0.002
3	0.1	0.1	0.008	0.011
4	1	1	0.05	0.043
5	5	5	0.04	0.137
6	10	10	0.02	0.071
7	20	20	0.02	0.141

Comb.	PTX (μM)	NuBCP-9 (μM)	FA	CI
1	0.001	0.001	0.51	0.007
2	0.01	0.01	0.3	0.014
3	0.1	0.1	0.13	0.02
4	1	1	0.09	0.093
5	5	5	0.04	0.094
6	10	10	0.02	0.05
7	20	20	0.02	0.10

Figure 5.

PTX is synergistic with NuBCP-9 in inhibiting breast cancer cell viability. (**A** and **B**) MCF-7 (**A**) and MDA-MB-231 (**B**) cells were treated with 10 nM PTX/NPs, 10 nM NuBCP-9/NPs, 10 nM each of PTX/NPs and NuBCP-9/NPs, and 10 nM of PTX-NuBCP-9/NPs for 72 h. Cell viability was determined by XTT assays. The results are presented as percentage viability (mean ± SD of 3 replicates). (**C** and **D**) MCF-7 (**C**) and MDA-MB-231 (**D**) cells were treated with the indicated concentrations of PTX/NPs alone, (2) the indicated concentrations of NuBCP-9/NPs alone and (3) indicated concentrations of PTX-NuBCP-9/NPs for 72 h. Mean cell survival was assessed in triplicate by XTT assays.

Numbers 1 to 7 in the graphs (left) represent combinations listed in tables (right). FA, fraction affected. CI, combination index.

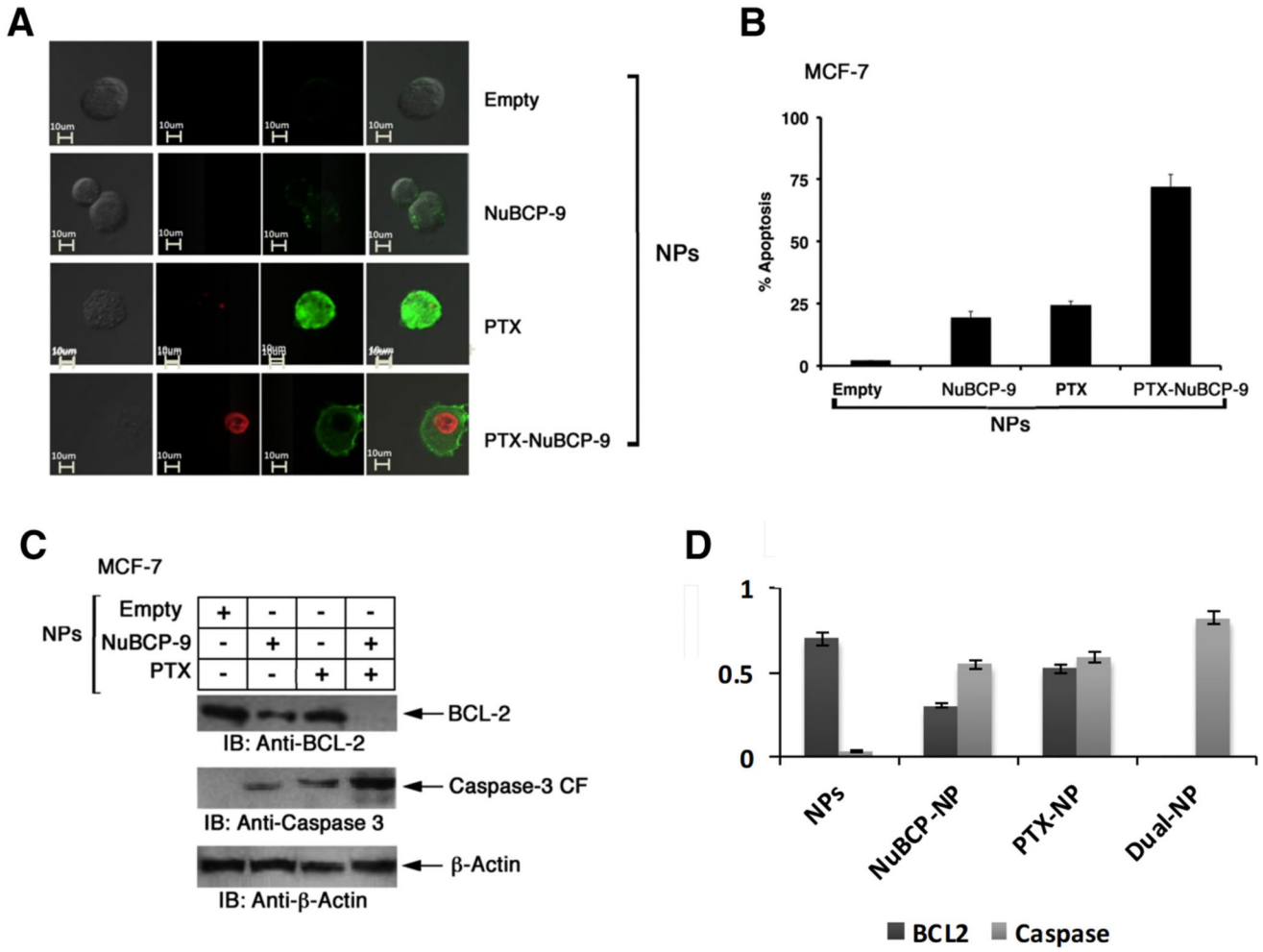

Figure 6.

Effects of NPs on induction of apoptosis. (**A**) Confocal laser scanning microscopic images of Annexin V/PI (Invitrogen, Molecular Probes, US) double staining of MCF-7 cells treated with empty NPs (top panel), NuBCP-9/NPs (second panel), PTX/NPs (third panel) and PTX-NuBCP-9/NPs (bottom panel) for 48 h. (**B**) MCF-7 cells were either treated with empty NPs, 1 M NuBCP-9/NPs, 100 nM PTX/NPs or 100 nM PTX-NuBCP-9/NPs for 48 h. Cells were stained with Annexin V/PI and analyzed by FACS. Results are presented as percentage apoptosis (mean ± SD of three replicates). (**C**) MCF-7 cells were treated with PBS (negative control), 1 M NuBCP-9/NPs, 100 nM PTX/NPs or 100 nM of PTX/NuBCP-9/NPs for 72 h. Whole cell lysates were analyzed by immunoblotting with the indicated antibodies. (**D**) Quantification of immunoblots using Image J software.

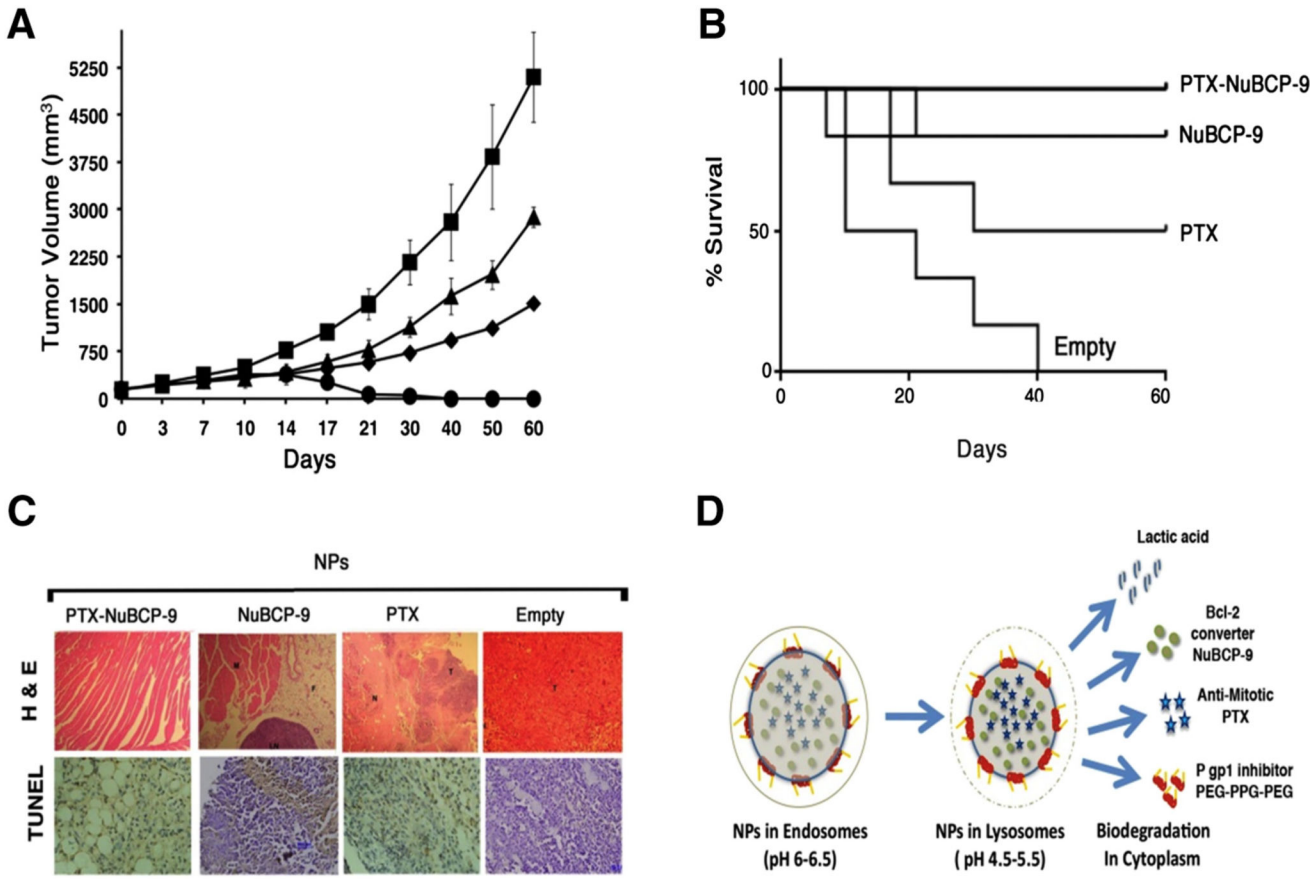

Figure 7.

Antitumor activity of PTX-NuBCP-9/NPs. (**A**) BALB/c mice (6 per group) with subcutaneous Ehrlich tumors (~150 mm^3) were treated IP with empty NPs (Squares), 10 mg/kg NuBCP-9 encapsulated NPs (IP, triangles, twice weekly), 10 mg/kg PTX encapsulated NPs (IP, diamonds, twice weekly) or 10 mg/kg PTX-NuBCP9 dual drug encapsulated NPs (IP, circles, twice weekly) for 3 weeks. Tumor measurements were performed on the indicated days. The results are expressed as tumor volumes (mean ± SD). (**B**) The results are expressed as the percentage survival as determined by Kaplan–Meier analysis for mice treated with empty NPs, NuBCP-9/NPs, PTX/NPs and PTX/NuBCP-9/NPs. The statistical analysis was performed between the empty NP control and the PTX-NuBCP-9/NP-treated group ($P < 0.001$). (**C**) Histopathology of tumor tissues obtained from mice treated with the empty NPs, PTX/NPs, NuBCP-9/NPs and PTX-NuBCP-9/NPs for 21 days and stained with hematoxylin and eosin (X400). (**D**) Schematic representation of the endosomal lyposomal cytoplasmic pH-dependent degradation of NPs and the release of different payloads.

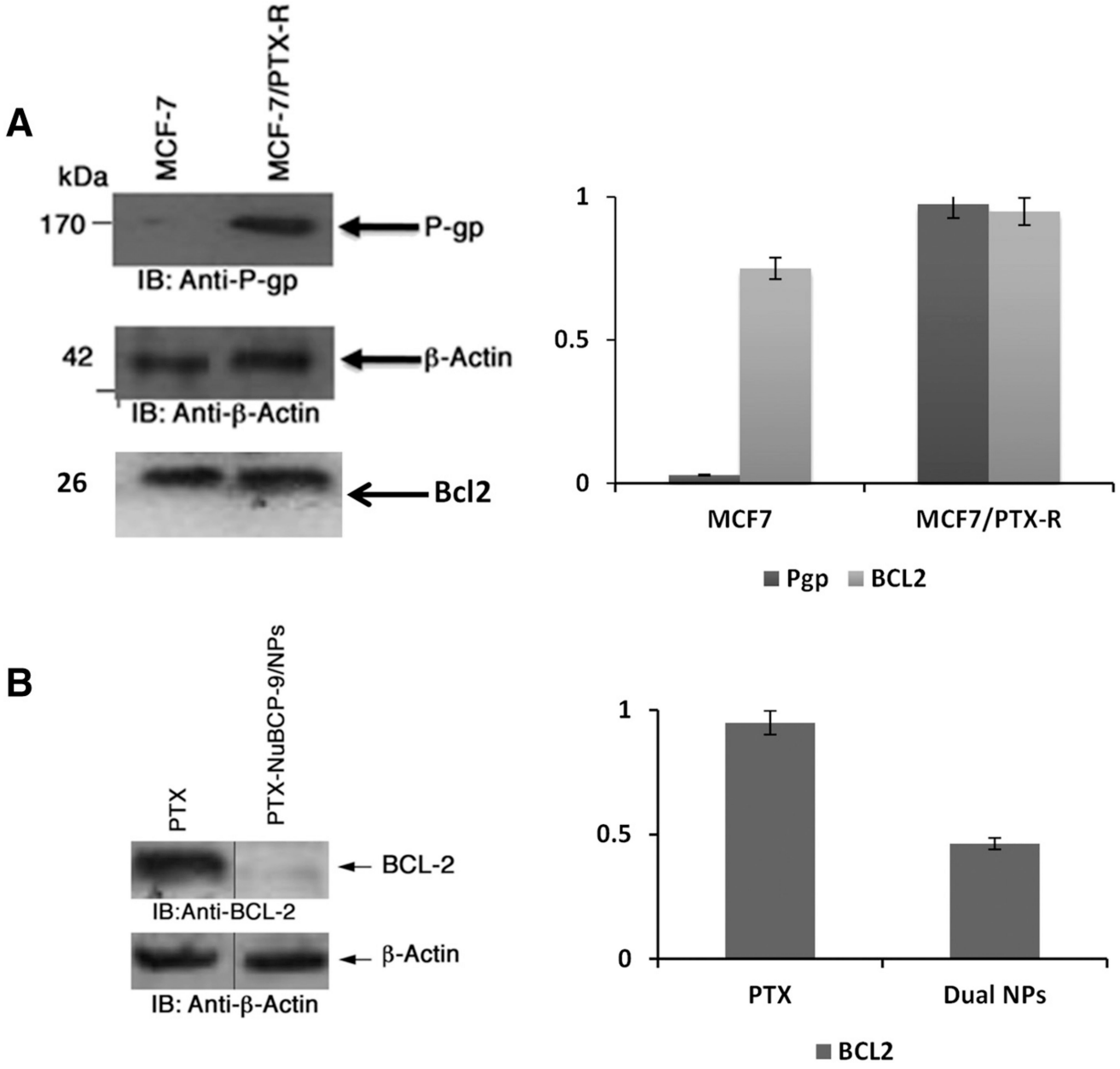

Figure 8.

Effects of NPs on PTX-resistant breast cancer cells. (**A**) Left panel. Whole cell lysates from MCF-7 and MCF-7/PTX-R analysed by immunobloting with anti P-gp1, anti-BCL2 and anti–actin antibodies. Right panel. Quantification of immunoblots using Image J software. (**B**) Left Panel. Whole cell lysates from MCF-7/PTX-R cells treated with 100 nM PTX/NPs and PTX-NuBCP-9/NPs for 72 h were analyzed by immunoblotting with anti-BCL-2 and anti-actin antibodies. Right panel. Quantification of immunoblots using Image J software for densitometry analysis of protein bands.

Table 1

Physiochemical characteristics of tetrablock PLA–PEG-PPG-PEG NPs.

Nanoparticles (NPs)	PTX:NuBCP-9 (w/w)	Drug/Polymer ratio	% EE PTX	% EE NuBCP-9	Size(nm)	Zeta Potential	PDI
PLA–PEG-PPG-PEG	–	–	–	–	104.0 ± 7.2	−17.9	0.09
NuBCP-9	0:1	1:10	–	64.61	130.1	−28.7	0.10
PTX	1:0	1:10	87.63	–	135.4	−3.21	0.12
PTX-NuBCP-9	3:1	1:10	96.84	12.74	172.0 ± 4.8	−8.57	0.11
PTX-NuBCP-9	1:1	1:10	98.96	20.01	165.1 ± 6.4	−9.23	0.01
PTX-NuBCP-9	1:3	1:10	99.19	28.77	160.1 ±9.1	−11.3	0.07

Table 2

IC50 values of different nanoformulation of NPs breast cancer cell lines.

Treatments	IC_{50} (nM)	
	MCF-7	MDA-MB-231
PTX	38	46
PTX/NPs	42.6	113
NuBCP-9/NPs	2000	3600
PTX/NPs + NuBCP-9/NPs	17	22
PTX-NuBCP-9/NPs	1	12

Table 3

IC_{50} values of PTX, nab-paclitaxel, PTX/NPs and PTX-NuBCP-9/NPs in MCF-7 and MCF-7/PTX-R cell lines.

	IC_{50} (μM)	
Treatment	**MCF-7**	**MCF-7/PTX-R**
PTX	0.027	1.75
PTX-NuBCP-9/NPs	0.002	0.01